
[View Journal Online](#)  
[View Article Online](#)

# Theoretical insights into the structural, spectroscopic, solvent effect, reactivity, NCI, and NLO analyses of 5,7-dichloro-8-hydroxyquinoline-2-carbaldehyde

 Ceyhun Kucuk \*

Ahmet Erdogan Vocational School of Health Services, Zonguldak Bulent Ecevit Univerity, Zonguldak, Turkey

 \* Corresponding author at: Ahmet Erdogan Vocational School of Health Services, Zonguldak Bulent Ecevit Univerity, Zonguldak, Turkey.  
 e-mail: [ceyhun.kucuk@beun.edu.tr](mailto:ceyhun.kucuk@beun.edu.tr) (C. Kucuk).

## RESEARCH ARTICLE



doi 10.5155/eurjchem.16.1.70-82.2634

 Received: 7 January 2025  
 Received in revised form: 19 January 2025  
 Accepted: 15 February 2025  
 Published online: 31 March 2025  
 Printed: 31 March 2025

## KEYWORDS

 NCI  
 DFT  
 NBO  
 Solvent effect  
 Vibrational spectra  
 8-Hydroxyquinoline

## ABSTRACT

In this study, the characterization of the 5,7-dichloro-8-hydroxyquinoline-2-carbaldehyde molecule was carried out by nuclear magnetic resonance ( $^1\text{H}$  and  $^{13}\text{C}$  NMR), Fourier transform infrared (FT-IR), ultraviolet-visible (UV-vis) spectroscopy and theoretical calculations in density functional theory (DFT) and time-dependent density functional theory (TD-DFT). The integral equation formalism polarizable continuum (IEFPCM) solvation model was used for ethanol, dimethylsulfoxide (DMSO), and water solvents. The conformation of the molecule was analyzed, and the most stable structure was optimized, and the geometry and electronic structure of the optimized structure were examined. The chemical stability and charge transport inside the molecule were validated by the computed HOMO-LUMO band gap energies. Characteristics such as non-linear optic properties (NLO), charge analysis, and molecular electrostatic potential (MEP) aid in determining the electrophilic/nucleophilic nature. Compound intermolecular interactions were investigated by topological studies, including noncovalent interaction (NCI), reduced density gradient (RDG), electron localization function (ELF), and localized orbital locator (LOL). The natural bond order (NBO) analysis was used to examine the changes between the hyperconjugative interaction energy  $E^{(2)}$  and the electron densities of the donor (i) and acceptor (j) bonds. The interaction energy, the NCI study, and the NBO analysis revealed that the ligand becomes stronger in the presence of a pyridine ring.

 Cite this: *Eur. J. Chem.* 2025, 16(1), 70-82

 Journal website: [www.eurjchem.com](http://www.eurjchem.com)

## 1. Introduction

5,7-Dichloro-8-hydroxyquinoline-2-carbaldehyde, a halogenated derivative of 8-hydroxyquinoline that functions as a bioactive metal chelator, was used for the first time as an antibiotic to treat diarrhea and skin infections [1]. Quinololin derivatives have long been used as active pharmaceutical ingredients in a variety of potent antibacterial, antifungal and antiamebic medicines used to treat dermatoses [2-4] as well as antiseptic or disinfectant formulations [5]. 8-Quinololin derivative drugs are also effective against viral and protozoal diseases by inhibiting deoxyribonucleic acid (DNA) replication. [6]. Furthermore, quinoline derivatives have gained recent attention from chemists due to their applicability in the synthesis of molecules with good nonlinear optical properties, use in organic light-emitting diodes and components of a variety of natural products [7].

Quinolones are used in medical applications, imaging reagents, and fluorescent reagents; they have a good electron mobility potential and good oxidative and thermal stability [8,9]. In a review of the literature, some halogen-substituted hydroxyquinoline structures have been elucidated with the help of quantum chemical calculations and experimental

methods [10]. However, there is no study explaining how the solvent affects the spectroscopic or electronic properties of the 5,7-dichloro-8-hydroxyquinoline-2-carbaldehyde molecule with quantum chemical calculation methods. Therefore, the aim of this study was to investigate how solvents affect the spectroscopic and electronic properties of the molecule. Therefore, calculations were performed using DFT to determine the vibrational properties, atomic charges, and reactivity of the title molecule. Furthermore, since the production of drugs and biological processes occurs in the solution phase, studying the effect of solvents on biomolecules is critical. As a result, we investigated the solute-solvent interactions of the therapeutic active ingredient structure at the molecular level. Using the IEFPCM model with DFT, we studied solvent effects on geometric structures, charge distribution, molecular electrostatic potential (MEP) surfaces, frontier molecular orbitals (FMO), FT-IR, NMR, and UV-vis spectra in the gas and solvent phases (water, DMSO, and EtOH).

## 2. Experimental

The Spartan 08 package program was used to perform a conformational analysis of the 5,7-dichloro-8-hydroxy quino-

**Table 1.** Geometric parameters of the 5,7-aichloro-8-hydroxyquinoline-2-carbaldehyde molecule.

Parameters	Bond lengths (Å)		Parameters	Bond angles (°)	
	6-311++G(d,p)	XRD *		6-311++G(d,p)	XRD *
Cl <sub>1</sub> -C <sub>9</sub>	1.758	1.823	C <sub>8</sub> -O <sub>3</sub> -H <sub>20</sub>	109.16	-
Cl <sub>2</sub> -C <sub>11</sub>	1.758	-	C <sub>7</sub> -N <sub>5</sub> -C <sub>14</sub>	118.61	117.04
O <sub>3</sub> -C <sub>8</sub>	1.343	1.330	C <sub>7</sub> -C <sub>6</sub> -C <sub>9</sub>	118.57	118.32
O <sub>3</sub> -H <sub>20</sub>	0.967	-	C <sub>7</sub> -C <sub>6</sub> -C <sub>10</sub>	117.10	116.99
O <sub>4</sub> -H <sub>15</sub>	1.208	-	C <sub>9</sub> -C <sub>6</sub> -C <sub>10</sub>	124.32	124.67
N <sub>5</sub> -C <sub>7</sub>	1.351	1.368	N <sub>5</sub> -C <sub>7</sub> -C <sub>6</sub>	122.28	123.26
N <sub>5</sub> -C <sub>14</sub>	1.319	1.322	N <sub>5</sub> -C <sub>7</sub> -C <sub>8</sub>	117.77	116.91
C <sub>6</sub> -C <sub>7</sub>	1.434	-	C <sub>6</sub> -C <sub>7</sub> -C <sub>8</sub>	119.94	119.83
C <sub>6</sub> -C <sub>9</sub>	1.419	1.425	O <sub>3</sub> -C <sub>8</sub> -C <sub>7</sub>	117.89	-
C <sub>6</sub> -C <sub>10</sub>	1.418	1.416	O <sub>3</sub> -C <sub>8</sub> -C <sub>11</sub>	123.87	-
C <sub>7</sub> -C <sub>8</sub>	1.434	1.427	C <sub>7</sub> -C <sub>8</sub> -C <sub>11</sub>	118.23	119.82
C <sub>8</sub> -C <sub>11</sub>	1.382	1.374	Cl <sub>1</sub> -C <sub>9</sub> -C <sub>6</sub>	120.30	119.58
C <sub>9</sub> -C <sub>12</sub>	1.371	1.363	Cl <sub>1</sub> -C <sub>9</sub> -C <sub>12</sub>	118.61	119.86
C <sub>10</sub> -C <sub>13</sub>	1.369	1.358	C <sub>6</sub> -C <sub>9</sub> -C <sub>12</sub>	121.08	120.54
C <sub>10</sub> -H <sub>16</sub>	1.082	-	C <sub>6</sub> -C <sub>10</sub> -C <sub>13</sub>	119.75	119.48
C <sub>11</sub> -C <sub>12</sub>	1.407	1.394	C <sub>6</sub> -C <sub>10</sub> -H <sub>16</sub>	119.24	-
C <sub>12</sub> -H <sub>17</sub>	1.081	-	C <sub>13</sub> -C <sub>10</sub> -H <sub>16</sub>	121.01	-
C <sub>13</sub> -C <sub>14</sub>	1.415	1.406	Cl <sub>2</sub> -C <sub>11</sub> -C <sub>8</sub>	118.68	-
C <sub>13</sub> -H <sub>18</sub>	1.083	-	Cl <sub>2</sub> -C <sub>11</sub> -C <sub>12</sub>	118.93	-
C <sub>14</sub> -C <sub>15</sub>	1.494	-	C <sub>8</sub> -C <sub>11</sub> -C <sub>12</sub>	122.39	119.95
C <sub>15</sub> -H <sub>19</sub>	1.106	-	C <sub>9</sub> -C <sub>12</sub> -C <sub>11</sub>	119.79	121.48
RMSD	0.02	-	C <sub>9</sub> -C <sub>12</sub> -H <sub>17</sub>	120.72	-
			C <sub>11</sub> -C <sub>12</sub> -H <sub>7</sub>	119.48	120.10
			C <sub>10</sub> -C <sub>13</sub> -C <sub>14</sub>	118.53	119.36
			C <sub>10</sub> -C <sub>13</sub> -H <sub>18</sub>	122.27	-
			C <sub>14</sub> -C <sub>13</sub> -H <sub>18</sub>	119.19	-
			N <sub>5</sub> -C <sub>14</sub> -C <sub>13</sub>	123.72	123.83
			N <sub>5</sub> -C <sub>14</sub> -C <sub>15</sub>	115.39	-
			C <sub>13</sub> -C <sub>14</sub> -C <sub>15</sub>	120.88	-
			O <sub>4</sub> -C <sub>15</sub> -C <sub>14</sub>	123.75	-
			O <sub>4</sub> -C <sub>15</sub> -H <sub>19</sub>	122.58	-
			C <sub>14</sub> -C <sub>15</sub> -H <sub>19</sub>	113.66	-
			RMSD	1.08	-

\* 5-Chloro-8-hydroxyquinoline [22].

line-2-carbaldehyde molecule using the MMFF (molecular mechanics approach) theory [11]. The Gaussian 09 package program [12,13] was used to calculate all other calculations in the study. In addition, the images corresponding to these calculations were obtained from the Gauss View 5.0 program [14]. The DFT/B3LYP/6-311++G(d,p) level of theory was used for optimization, frequency, UV-vis, electronic, and optical properties calculations [15]. UV-vis calculations were performed for ethanol, DMSO, and water solvent. The IEFPCM model, the gauge-including atomic orbital (GIAO) method and the 6-311+G(2d,p) basis set were used to perform NMR calculations for ethanol, DMSO, and water solvents [16,17].

For the 5,7-dichloro-8-hydroxyquinoline-2-carbaldehyde molecule, a graph has been plotted with respect to the total density of state (TDOS), the partial density of state (PDOS), and the overlap population density of state (OPDOS). The graph was plotted with the aid of a multiifwn analyzer, which examined and translated the main contribution of each set of molecular orbitals [18]. Furthermore, electron localization function (ELF) and localized orbital locator (LOL) surface maps were produced using the Multiwfn program [18].

### 3. Results and discussion

#### 3.1. Conformational analysis and optimization calculations

Before optimization calculations are performed, conformer analysis is a crucial step in determining the most thermodynamically stable structure of a molecule based on torsional angles [19-21]. Using the MMFF theory and the molecular mechanics approach, we conducted conformational analyses of the title molecule in the Spartan 08 package program [11]. As a result of the calculations, two conformer structures were found. These structures are given in Figure 1 with energy and Boltzmann distribution values. Since the Boltzmann distribution for the conformer I structure was found to be 1.00 and the energy value was found to be 3.13 eV, optimization

calculations were performed for this structure. In addition, the optimized conformer I structure was used in the calculations performed for spectroscopic and electronic properties. The optimized structure is presented in Figure 2. The values of the bond lengths and bond angles are listed in Table 1. Furthermore, the calculated values were compared with the bond length and bond angle values obtained from the X-ray diffraction (XRD) data of the 5-chloro-8-hydroxyquinoline molecule [22].

The bond lengths of O<sub>3</sub>-C<sub>8</sub> and O<sub>4</sub>=C<sub>15</sub> were calculated as 1.343 and 1.208 Å, while the O<sub>3</sub>-C<sub>8</sub> bond length for the 5-chloro-8-hydroxyquinoline molecule was reported as 1.330 Å [22]. The bond lengths for N<sub>5</sub>-C<sub>7</sub> and N<sub>5</sub>-C<sub>14</sub> were 1.351 and 1.319 Å, while these values for the crystal structure of the given example were 1.368 and 1.322 Å [22]. The bond lengths for Cl<sub>1</sub>-C<sub>9</sub> and Cl<sub>2</sub>-C<sub>11</sub> formed by Cl atoms at positions 5 and 7 of the title molecule were calculated as 1.758 Å. The bond length of Cl<sub>1</sub>-C<sub>9</sub> in the structure presented for comparison is 1.823 Å [22]. The bond length values of the carbon atoms in the ring were calculated to be very close to the values of the molecule presented for comparison.

The bond angles of O<sub>3</sub>-C<sub>8</sub>-C<sub>7</sub>, O<sub>3</sub>-C<sub>7</sub>-C<sub>11</sub>, and O<sub>4</sub>-C<sub>15</sub>-C<sub>14</sub> were calculated as 117.89, 123.87, and 123.75°, respectively. Although the C<sub>7</sub>-N<sub>5</sub>-C<sub>14</sub> bond angle was found to be 118.61° in theoretical calculations, this angle value was reported as 117.04° for 5-chloro-8-hydroxyquinoline XRD data [22]. The Cl<sub>1</sub>-C<sub>9</sub>-C<sub>6</sub> and Cl<sub>1</sub>-C<sub>9</sub>-C<sub>12</sub> angles were calculated as 120.30 and 118.61°, and these angle values were measured as 119.58 and 119.86° in the XRD data of the sample molecule [22]. The Cl<sub>2</sub>-C<sub>11</sub>-C<sub>8</sub> and Cl<sub>2</sub>-C<sub>11</sub>-C<sub>12</sub> bond angles were calculated as 118.68 and 118.93°.

In addition, the values in the XRD data of the sample molecule in the ring angles were calculated quite closely. Root mean square deviation (RMSD) values were calculated to show the agreement between the length of the bond and the angles of the bond, and this value was found to be 0.02 for the length of the bond and 1.08 for the angles of the bond. In other words, it can be said that they are quite compatible with each other.

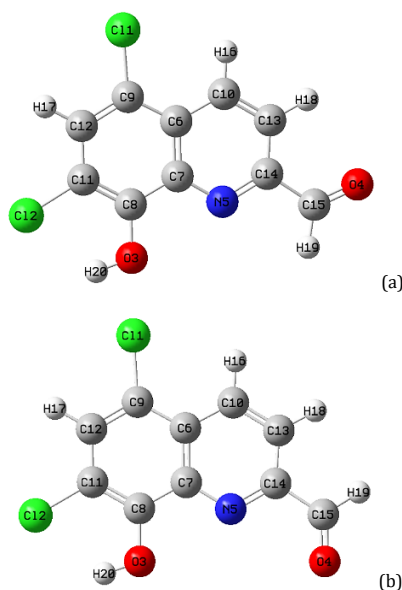


**Figure 1.** Conformer I ( $E = 3.13$  eV) (a) and Conformer II ( $E = 3.52$  eV) (b) structures of the 5,7-dichloro-8-hydroxyquinoline-2-carbaldehyde molecule.

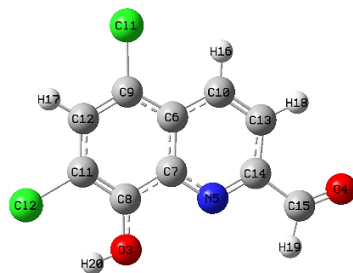


**Figure 2.** Optimized geometric structure of the 5,7-dichloro-8-hydroxyquinoline-2-carbaldehyde molecule.

### 3.2. Frequency analysis

Frequency analysis was performed for the optimized structure of the title molecule. The calculated wavenumbers in the gas phase and their corresponding mode values are listed in Table 2. The scale factor was not used for the calculated wavenumbers in the gas phase and solvents. Furthermore, the shift amounts between the frequency values calculated in the solvents and the values calculated in the gas phase are also given in Table 2. The IR spectra obtained from the calculations are presented in Figure 3. The amount of shift in the frequency values is obtained with the formula below (Equation 1).

$$\Delta\nu = \Delta\nu_{\text{gas}} - \Delta\nu_{\text{solvent}} \quad (1)$$

The OH stretching vibration was calculated at  $3756\text{ cm}^{-1}$ . According to the literature, these vibration modes are also assigned to the region  $3400\text{--}3800\text{ cm}^{-1}$  [23]. In the calculations performed in the IEFPCM model, this stretching vibration peak shifted to a smaller value of  $15\text{ cm}^{-1}$  in the ethanol solvent and  $16\text{ cm}^{-1}$  in the water solvent. For the 5-chloro-8-hydroxyquinoline molecule, which is structurally similar to the title molecule, this vibrational value was observed at  $3465\text{ cm}^{-1}$  [24].

The C-H stretching vibrations of hetero-aromatic compounds are detected between  $3100$  and  $3000\text{ cm}^{-1}$  [25,26]. A total of four C-H stretching vibrations were calculated for the title molecule. According to the calculations in the gas phase, two symmetric stretching vibrations at  $3214$  and  $3212\text{ cm}^{-1}$ , one asymmetric stretching vibration at  $3199\text{ cm}^{-1}$ , and one C-H stretching vibration belonging to the carbaldehyde group at

$2953\text{ cm}^{-1}$  were obtained. In all solvents, a shift of  $-3$ ,  $-5$ ,  $-6$ , and  $-12\text{ cm}^{-1}$  occurred in these four frequency values, respectively. They were calculated at  $3217$ ,  $3217$ ,  $3205$ , and  $2965\text{ cm}^{-1}$ . C-H stretching vibrations were reported for the 5-chloro-8-hydroxyquinoline molecule at  $3093$ ,  $3065$ , and  $3030\text{ cm}^{-1}$  [24].

The C=O stretching vibration occurs at a frequency of  $1900\text{--}1725\text{ cm}^{-1}$  [27]. In the gas phase calculations, the C=O stretching vibration assigned at  $1776\text{ cm}^{-1}$  shifted to a smaller value of  $29\text{ cm}^{-1}$  ( $1747\text{ cm}^{-1}$ ) in the ethanol solvent and  $30\text{ cm}^{-1}$  ( $1746\text{ cm}^{-1}$ ) in the DMSO and water solvents. The C-O stretching vibrations were calculated at  $1417$  and  $1236\text{ cm}^{-1}$  in the gas phase. The calculated value at  $1417\text{ cm}^{-1}$  shifted to  $1415\text{ cm}^{-1}$  in all solvent calculations, while the calculated value at  $1236\text{ cm}^{-1}$  shifted to  $1232\text{ cm}^{-1}$ . The C-O stretching vibration of the 5-chloro-8-hydroxyquinoline molecule was observed at  $1225\text{ cm}^{-1}$  in the experimental IR spectrum [24].

The ring C-C stretching vibrations are mostly seen between  $1650$  and  $1200\text{ cm}^{-1}$  [28]. The C-C stretching vibrations were calculated for the gas phase at  $1622$ ,  $1591$ ,  $1528$ ,  $1417$ ,  $1395$ ,  $1376$ ,  $1355$ ,  $1271$ , and  $1211\text{ cm}^{-1}$ . Examining Table 2 for these stretching vibrations revealed that there were no shifts at certain frequency values for the solvent calculations and showed that the largest shift value was  $4\text{ cm}^{-1}$ . The C-C stretching vibrations of the 5-chloro-8-hydroxyquinoline molecule were observed in the IR spectrum at  $1599$ ,  $1565$ ,  $1467$ , and  $1392\text{ cm}^{-1}$  [24].

The C-N stretching vibration modes are observed in the range of  $1342\text{--}1266\text{ cm}^{-1}$  in the IR spectrum [29]. While the C-N stretching vibrations were calculated at  $1633$  and  $1489\text{ cm}^{-1}$  for the gas phase, for three solvents, these two frequency values

**Table 2.** Calculated frequency values with the total energy densities of the 5,7-dichloro-8-hydroxyquinoline-2-carbaldehyde molecule.

Mode	Frequency( $\nu$ )				$I_{IR}^a$	TED <sup>b,c</sup>
	Gas $\epsilon = 1$	$\Delta\nu$ Ethanol $\epsilon = 24.3$	$\Delta\nu$ DMSO $\epsilon = 46.8$	$\Delta\nu$ Water $\epsilon = 78.3$		
1	61	-3	-3	-3	0.31	41 $\Gamma_{CCCC}$ + 36 $\Gamma_{ClCCC}$
2	85	-1	-1	-1	0.31	69 $\Gamma_{CCCO}$
3	122	0	0	0	0.82	11 $\Gamma_{CCCC}$ + 62 $\Gamma_{ClCCC}$
4	135	0	0	0	0.41	60 $\delta_{CCC}$
5	144	0	0	0	0.47	62 $\Gamma_{CCCN}$
6	192	1	1	1	0.07	85 $\delta_{ClCC}$
7	240	1	1	1	4.14	62 $\Gamma_{CCCC}$
8	255	2	2	2	1.13	61 $\delta_{OCC}$ + 12 $\Gamma_{ClCCC}$
9	279	0	0	0	0.20	11 $\delta_{CCC}$ + 15 $\Gamma_{CCCN}$ + 27 $\Gamma_{ClCCC}$
10	302	-2	-2	-2	3.81	12 $\delta_{CCC}$ + 12 $\delta_{OCC}$
11	337	0	0	0	2.90	31 $\nu_{ClC}$ + 18 $\delta_{CCC}$
12	368	0	0	0	0.32	46 $\nu_{ClC}$ + 12 $\delta_{CCC}$
13	371	-3	-3	-3	0.09	57 $\Gamma_{CNCC}$
14	415	-1	-1	-1	0.21	41 $\delta_{CCC}$ + 10 $\delta_{CCN}$
15	433	6	6	6	11.42	69 $\Gamma_{CCH}$
16	453	7	7	7	11.72	79 $\Gamma_{CNCC}$
17	545	-4	-4	-4	3.27	54 $\Gamma_{CCCC}$
18	575	-1	-1	-1	0.88	12 $\delta_{CNC}$ + 11 $\delta_{CCC}$ + 111 $\delta_{CCO}$ + 22 $\delta_{ClCC}$
19	609	-2	-2	-2	0.01	69 $\Gamma_{CCCC}$
20	619	0	0	0	2.52	32 $\delta_{CCC}$
21	633	0	0	0	1.17	44 $\delta_{ClCC}$
22	686	-9	-9	-9	0.61	69 $\Gamma_{CCCN}$
23	720	2	2	2	6.15	14 $\nu_{ClC}$ + 18 $\delta_{CCN}$
24	738	4	4	4	14.53	36 $\nu_{CC}$ + 20 $\delta_{CCC}$
25	792	3	3	3	28.85	23 $\nu_{CC}$ + 10 $\nu_{ClC}$ + 27 $\delta_{CCN}$
26	809	-7	-7	-7	0.56	62 $\Gamma_{CCCC}$
27	856	3	4	4	5.59	75 $\Gamma_{CCH}$
28	883	-8	-8	-8	6.83	79 $\Gamma_{CCH}$
29	949	-1	-1	-1	9.00	16 $\delta_{CCC}$
30	960	4	4	4	17.11	13 $\nu_{ClC}$ + 40 $\delta_{CCC}$
31	1016	-2	-2	-2	0.19	72 $\Gamma_{CCH}$
32	1026	-2	-2	-2	0.29	11 $\Gamma_{CCCC}$ + 73 $\Gamma_{CCH}$
33	1096	4	4	4	12.94	14 $\nu_{CC}$ + 32 $\delta_{CNC}$
34	1158	3	3	3	1.52	55 $\delta_{CCH}$
35	1211	0	0	0	1.24	12 $\nu_{CC}$ + 14 $\delta_{HOC}$ + 32 $\delta_{CCH}$
36	1236	4	4	4	14.95	15 $\nu_{OC}$ + 17 $\delta_{CCH}$
37	1252	4	4	4	2.86	50 $\nu_{CC}$ + 15 $\delta_{CCH}$ + 12 $\delta_{HCN}$ + 11 $\delta_{CCH}$
38	1271	0	0	0	34.21	22 $\nu_{CC}$ + 10 $\delta_{CNC}$ + 14 $\delta_{HOC}$
39	1348	-2	-1	-1	0.64	11 $\nu_{CN}$ + 12 $\delta_{HOC}$ + 29 $\delta_{HCO}$
40	1355	4	4	4	17.99	57 $\nu_{CC}$
41	1376	0	0	0	20.40	22 $\nu_{CC}$ + 44 $\delta_{HCO}$
42	1395	0	0	0	15.71	11 $\nu_{CC}$ + 44 $\delta_{HOC}$
43	1417	2	2	2	12.40	12 $\nu_{CC}$ + 16 $\nu_{OC}$ + 33 $\delta_{HCC}$
44	1489	8	8	8	34.49	25 $\nu_{CN}$
45	1528	3	3	3	2.69	20 $\nu_{CC}$ + 12 $\delta_{HCC}$
46	1591	3	3	3	2.90	45 $\nu_{CC}$ + 12 $\delta_{CNC}$
47	1622	2	2	2	22.06	45 $\nu_{CC}$
48	1633	4	4	4	2.18	44 $\nu_{CN}$ + 10 $\nu_{CC}$
49	1776	29	30	30	100.00	92 $\nu_{OC}$ (O=C)
50	2953	-12	-12	-12	18.85	100 $\nu_{CH}$ (carbaldehyde)
51	3199	-6	-6	-6	0.28	100 $\nu_{CH}$ (asym)
52	3212	-5	-5	-5	0.25	99 $\nu_{CH}$ (sym)
53	3214	-3	-3	-3	0.71	100 $\nu_{CH}$ (sym)
54	3756	15	16	16	35.91	100 $\nu_{OH}$

<sup>a</sup> Relative absorption intensities normalized with highest peak absorption equal to 100.

<sup>b</sup> The total energy distribution level (TED) less than 10% is not shown.

<sup>c</sup>  $\nu$ : stretching,  $\delta$ : in-plane bending,  $\gamma$ : out-of bending  $\Gamma$ : torsion, s: strong, m: medium, w: weak, v: very.

were calculated at 1629 and 1481  $\text{cm}^{-1}$ . A shift of 4 and 8  $\text{cm}^{-1}$  occurred in the frequency values, respectively.

In general, the computed IR peaks become more pronounced as they transition from the gas phase to the solution. This is due to the fact that the solute's dipole moment is increased by the enhanced solvent polarity. As the solvent polarity increases, the vibrational frequencies of certain modes are shifted, and the corresponding IR intensities also undergo a change [30]. The significant change in IR intensities belongs to the C=O stretching vibration observed in the 49<sup>th</sup> mode. In addition, the largest shifts in wavenumbers belong to the 49<sup>th</sup>, 54<sup>th</sup>, and 50<sup>th</sup> modes, respectively.

### 3.3. <sup>1</sup>H and <sup>13</sup>C NMR analyses

<sup>1</sup>H and <sup>13</sup>C NMR chemical shift values for the optimized title molecule geometric structure were calculated using the gauge-including atomic orbital (GIAO) method and the IEFPCM model

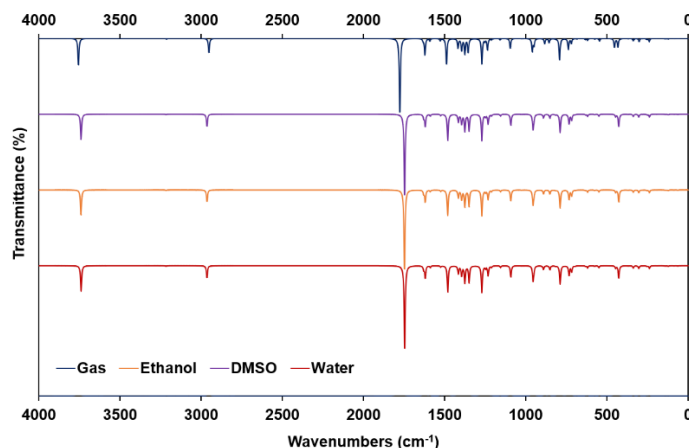
with the 6-311+(2d,p) basis set for ethanol, DMSO, and water solvents [17]. The results (Table 3) indicate that the <sup>13</sup>C NMR chemical shift of the typical organic molecule is typically calculated in the region of  $\delta$  10-200 ppm [31]. The highest chemical shift value among the C atoms belongs to the C<sub>15</sub> atom of the carbaldehyde group and was calculated as  $\delta$  203.44 ppm in the ethanol solution,  $\delta$  203.54 ppm in the DMSO solution, and  $\delta$  203.14 ppm in the water solution. The smallest chemical shift value was obtained for the C<sub>13</sub> atom and was found to be  $\delta$  123.16, 123.17, and 123.21 ppm for the solvents. For ethanol, DMSO, and water solutions, the chemical shift values for the C<sub>8</sub> and C<sub>14</sub> atoms are  $\delta$  156.48/156.43/155.63 ppm and  $\delta$  156.88/156.87/156.57 ppm, respectively. Chemical shift values for the C<sub>6</sub>, C<sub>7</sub>, C<sub>9</sub>, C<sub>10</sub>, C<sub>11</sub> and C<sub>12</sub> atoms are  $\delta$  133.59, 145.16, 134.17, 140.71, 130.00, and 135.82 ppm in ethanol solution, and  $\delta$  133.74, 145.16, 134.18, 140.78, 130.05, 135.89 ppm and  $\delta$  133.04, 146.47, 134.08, 140.16, 129.15, and 135.54 ppm in DMSO solution.

**Table 3.** Calculated  $^1\text{H}$  and  $^{13}\text{C}$  NMR chemical shift values of the 5,7-dichloro-8-hydroxyquinoline-2-carbaldehyde molecule.

Atoms	Ethanol $\epsilon = 24.3$	DMSO $\epsilon = 46.8$	Water $\epsilon = 78.3$	Atoms	Ethanol $\epsilon = 24.3$	DMSO $\epsilon = 46.8$	Water $\epsilon = 78.3$
H <sub>16</sub>	9.02	9.02	8.78	C <sub>6</sub>	133.59	133.74	133.04
H <sub>17</sub>	8.13	8.13	7.94	C <sub>7</sub>	145.16	145.16	146.67
H <sub>18</sub>	8.53	8.53	8.44	C <sub>8</sub>	156.48	156.46	155.63
H <sub>19</sub>	10.62	10.62	10.39	C <sub>9</sub>	134.17	134.18	134.08
H <sub>20</sub>	6.20	6.22	6.25	C <sub>10</sub>	140.71	140.78	140.16
				C <sub>11</sub>	130.00	130.05	129.95
				C <sub>12</sub>	135.82	135.89	135.54
				C <sub>13</sub>	123.16	123.17	123.21
				C <sub>14</sub>	156.88	156.87	156.57
				C <sub>15</sub>	203.44	203.54	203.14

**Table 4.** Energy values of quantum chemical properties of molecule 5,7-dichloro-8-hydroxyquinoline-2-carbaldehyde molecule.

Parameters	Energy Values (eV)			
	Gas $\epsilon = 1$	Ethanol $\epsilon = 24.3$	DMSO $\epsilon = 46.8$	Water $\epsilon = 78.3$
$E_{\text{HOMO}}$	-2.89	-2.89	-2.89	-2.89
$E_{\text{LUMO}}$	-6.71	-6.57	-6.57	-6.57
Energy band gap ( $\Delta E = E_{\text{LUMO}} - E_{\text{HOMO}}$ )	3.83	3.69	3.69	3.69
Ionization potential ( $I = -E_{\text{HOMO}}$ )	6.71	6.57	6.57	6.57
Electron affinity ( $A = -E_{\text{LUMO}}$ )	2.89	2.89	2.89	2.89
Chemical hardness ( $\eta = (-E_{\text{HOMO}} + E_{\text{LUMO}})/2$ )	1.91	1.84	1.84	1.84
Chemical softness ( $\sigma = 1/2\eta$ )	0.52	0.54	0.54	0.54
Electronegativity ( $\chi = -\mu_c$ )	4.80	4.73	4.73	4.73
Chemical potential ( $\mu_c = (E_{\text{HOMO}} + E_{\text{LUMO}})/2$ )	-4.80	-4.73	-4.73	-4.73
Global electrophilicity ( $\omega = \mu_c^2/2\eta$ )	6.02	6.07	6.07	6.07

**Figure 3.** Calculated IR spectrum of the 5,7-dichloro-8-hydroxyquinoline-2-carbaldehyde molecule.

The aromatic proton signals of the organic molecules are observed around  $\delta$  6.20-8.20 ppm [32]. Chemical shift values for H<sub>16</sub>, H<sub>17</sub>, H<sub>18</sub> and H<sub>19</sub> atoms were calculated as  $\delta$  9.02, 8.13, 8.53 and 10.62 ppm for ethanol and DMSO solutions, respectively. In water solution, they were calculated as  $\delta$  8.78, 7.94, 8.44 and 10.39 ppm. The chemical shift values for the H<sub>20</sub> atom are  $\delta$  6.20, 6.22, and 6.25 ppm. When NMR calculations made in different solvents are compared with each other, the chemical shift values for H atoms are found to be the same in ethanol and dimethyl sulfoxide solvents, while the chemical shift values shifted to smaller values in the water solvent, which has the highest dielectric constant. Similar results were obtained for C atoms.

### 3.4. Frontier molecular orbitals (FMOs)

Frontier molecular orbitals play a crucial role in determining the chemical reactivity, electron-donating, and accepting abilities of molecular systems [33,34]. Figure 4 illustrates the frontier molecular orbital, while Table 4 displays the quantum-chemical parameters. The HOMO-LUMO energy gap is calculated using differences of 3.83, 3.58, 3.58, and 3.58 eV for gas, ethanol, DMSO, and water as solvents. This demonstrates small changes in the band gap energy for the solvent dielectric constant, which is consistent with the Stokes shifts [35]. The energy gap values observed indicate the

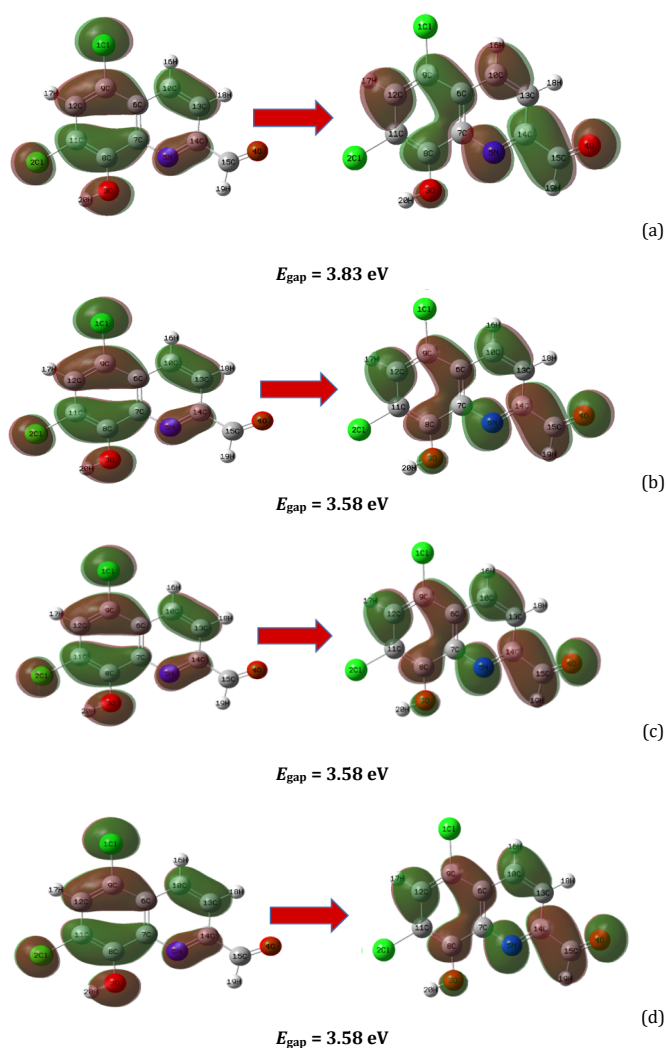
stability and bioactivity of the 5,7-dichloro-8-hydroxyquinoline-2-carbaldehyde molecule, as well as the occurrence of charge transfer within them. The chemical hardness, calculated at 1.91 eV, indicates the compound's stability, while the electronegativity (4.80 eV) defines the ability to induce shared electrons and predicts the attraction of electrons in a covalent bond. Furthermore, the chemical softness value of 0.52 eV reveals the ligand's non-toxic nature. These values showed very small decreases in the solvents.

### 3.5. Total partial and overlap population density-of-states

In the fields of solid-state physics and condensed matter physics, the Density of States (DOS) provides information about the distribution of states that can be held by a system at different energy levels [36]. The related graphs in Figure 5 were critical tools for describing the full orbitals of the system using Total Density of States (TDOS), which comprises the whole system with the help of partial PDOS. Furthermore, research on the character of chemical bonds was conducted using Density-of-States Superposition (OPDOS) diagrams, the sign of the OPDOS value being significant for discovering the type of contacts between orbitals, atomic groups, or atoms [37]. The highest occupied molecular orbital (HOMO) in this figure is represented by the vertical dashed line, which has an energy range of 0.20 to 0.30 a.u.

**Table 5.** Theoretical UV-Vis parameters of the 5,7-dichloro-8-hydroxyquinoline-2-carbaldehyde molecule.

Solvent	Theoretical				
	$\lambda$ (nm)	E (eV)	f	Symmetry	Major Contributions
Ethanol	221	5.614	0.6413	Singlet-A	HOMO-2 $\rightarrow$ LUMO+1 HOMO $\rightarrow$ LUMO+2
	273	4.541	0.815	Singlet-A	HOMO-2 $\rightarrow$ LUMO HOMO $\rightarrow$ LUMO+1
	395	3.143	0.696	Singlet-A	HOMO $\rightarrow$ LUMO
DMSO	221	5.603	0.6531	Singlet-A	HOMO-1 $\rightarrow$ LUMO+1 HOMO $\rightarrow$ LUMO+2
	273	4.526	0.8354	Singlet-A	HOMO-1 $\rightarrow$ LUMO HOMO $\rightarrow$ LUMO+1
	395	3.136	0.0702	Singlet-A	HOMO $\rightarrow$ LUMO
Water	221	5.619	0.6358	Singlet-A	HOMO-1 $\rightarrow$ LUMO+1 HOMO $\rightarrow$ LUMO
	273	4.542	0.8037	Singlet-A	HOMO-1 $\rightarrow$ LUMO HOMO $\rightarrow$ LUMO+1
	395	3.138	0.0665	Singlet-A	HOMO $\rightarrow$ LUMO

**Figure 4.** Description of the electron transition from the HOMO orbital to the LUMO orbital of the 5,7-dichloro-8-hydroxyquinoline-2-carbaldehyde molecule. (a) Gas phase, (b) Ethanol, (c) DMSO, (d) Water.

The DOS plot is compatible with the FMO's HOMO and LUMO energy differences. Both bonding and antibonding interactions are present in the HOMO molecular; the PDOS spectra's molecular orbital demonstrates that the pyridine benzene ring fragment's orbital contribution was greater than that of the pyridine ring and carbaldehyde group fragments. However, the LUMO molecular orbitals with antibonding interactions are the most dominant in the PDOS spectra of the pyridine ring.

### 3.6. UV-vis analysis

The UV-vis spectra of the title molecule were calculated in ethanol, dimethylsulfoxide (DMSO), and water solvents. Figure 6 displays the theoretical UV-vis spectra. Additionally, Table 5 presents the calculated maximum wavelengths, excitation energy values, oscillator strength, and main contribution values. The experimental spectra of the free ligand exhibited wavelengths at 287, 246, and 215 nm.

**Table 6.** The second order perturbation energies  $E^{(2)}$  (kcal/mol) corresponding to the most important charge transfer interactions (donor-acceptor) in the compound studied by the B3LYP/6-311++G(d,p) method in gas phase.

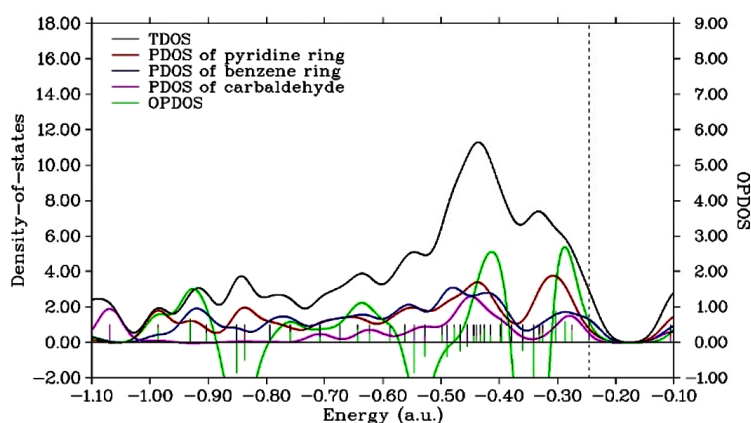
Donor NBO (i) <sup>a</sup>	Acceptor NBO (j)	$E^{(2)}$ (kcal/mol) <sup>b</sup>	$\epsilon_j - \epsilon_i$ (a.u.) <sup>c</sup>	$F_{(ij)}$ (a.u.) <sup>d</sup>
$\pi(N_5-C_{14})$	$\pi^*(O_4-C_{15})$	12.81	0.33	0.061
	$\pi^*(C_6-C_7)$	20.19	0.32	0.076
	$\pi^*(C_{10}-C_{13})$	11.38	0.34	0.056
$\pi(C_6-C_7)$	$\pi^*(N_5-C_{14})$	16.90	0.27	0.062
	$\pi^*(C_8-C_{11})$	19.06	0.26	0.064
	$\pi^*(C_9-C_{12})$	16.58	0.27	0.062
$\pi(C_8-C_{11})$	$\pi^*(C_{10}-C_{13})$	15.73	0.29	0.064
	$\pi^*(C_6-C_7)$	12.66	0.31	0.058
	$\pi^*(C_9-C_{12})$	20.56	0.30	0.072
$\pi(C_9-C_{12})$	$\pi^*(C_6-C_7)$	16.81	0.30	0.067
	$\pi^*(C_8-C_{11})$	13.99	0.29	0.059
	$\pi^*(N_5-C_{14})$	23.72	0.28	0.073
$\pi(C_{10}-C_{13})$	$\pi^*(C_6-C_7)$	17.07	0.28	0.065
	$\pi^*(C_9-C_{12})$	12.60	0.33	0.061
	$\pi^*(C_8-C_{11})$	11.45	0.33	0.060
LP(3)Cl	RY*(H <sub>20</sub> )	42.92	0.44	0.127
	$\pi^*(C_8-C_{11})$	35.90	0.33	0.103
	$\pi^*(C_{15}-H_{19})$	17.59	2.14	0.177
LP(2)O <sub>3</sub>	$\pi^*(C_{14}-C_{15})$	18.94	0.69	0.103
	$\pi^*(O_4-C_{15})$	122.91	0.01	0.072
	$\pi^*(C_{10}-C_{13})$	112.67	0.02	0.082
$\pi^*(N_5-C_{14})$	$\pi^*(C_{10}-C_{13})$	136.25	0.02	0.078

<sup>a</sup>  $\pi$ : pi bonds, LP: Lone pairs, RY\*: Rydberg.

<sup>b</sup>  $E^{(2)}$  means the energy of hyper-conjugative interactions.

<sup>c</sup> Energy difference between donor and acceptor i and j NBO orbitals.

<sup>d</sup>  $F_{(ij)}$  is the Fock matrix element between the i and j NBO orbitals.

**Figure 5.** Variation of OPDOS and TDOS, as well as PDOS in terms of energy (a.u.).

The main contributions for the absorption peak at 395 nm are due to the HOMO/LUMO transition for all three solutions. For the peak at 273 nm, these contributions are due to the HOMO-1/LUMO and HOMO/LUMO+1 transitions for DMSO and water solvents, while in the ethanol solvent, this contribution comes from the HOMO-2/LUMO and HOMO/LUMO+1 transitions. The main contribution values for 221 nm come from the HOMO-2/LUMO+1 and HOMO/LUMO+2 transitions in the ethanol solvent, the HOMO-1/LUMO+1 and HOMO/LUMO+2 transitions in the DMSO solvent and the HOMO-1/LUMO+1 and HOMO/LUMO transitions in the water solvent. In calculations made in different solvents, the wavelengths of the peaks observed in the UV-vis absorption spectrum did not change. In other words, the change in the dielectric constant in the medium did not cause any change in the wavelength.

### 3.7. Natural bond orbital (NBO) study

The analysis of natural bond orbitals (NBOs) is a valuable method to identify the properties of electronic systems [38-40]. The donor-acceptor interaction is distinguished by a stabilization energy  $E^{(2)}$  according to the NBO analysis. Table 6 shows the significant interactions with the highest stabilization

energies. The electron coupling  $\pi^*(C_6-C_7) \rightarrow \pi^*(C_{10}-C_{13})$ ,  $\pi^*(N_5-C_{14}) \rightarrow \pi^*(O_4-C_{15})$ ,  $\pi^*(N_5-C_{14}) \rightarrow \pi^*(C_{10}-C_{13})$  in the ligand constituted the most crucial transitions of energy. These interactions resulted in stabilization energies of 136.25, 122.91, and 112.67 kcal/mol, respectively. According to the second-order perturbation energy results, these electron transfers occurring in the pyridine ring constitute the main source of electron transitions in this molecule. Furthermore, the lone pair electrons between LP3(Cl) and LP2(O<sub>4</sub>) show that the chlorine and oxygen atoms contribute electrons to other bonds.

### 3.8. NCI-RDG analysis

The noncovalent interactions (NCI) visualization index is based on the density and its many components. These changes facilitate the identification of noncovalent interactions. The presence of reduced density gradient (RDG) peaks at low densities provides corroboration. These places create a substantial alteration in the RDG by eliminating the molecular density gradient [41]. In the scattering of the 5,7-dichloro-8-hydroxyquinoline-2-carbaldehyde molecule and the gradient isosurface map, there are several spikes between 0.05 and +0.05 a.u., which helped to explain the characteristics of the intermolecular interaction. Within the pyridine and benzene

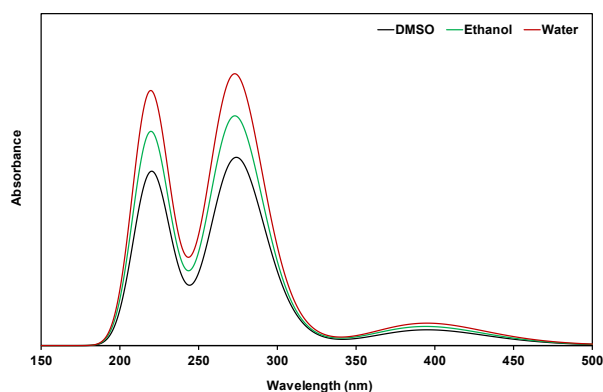


Figure 6. UV-vis absorption spectra of the 5,7-dichloro-8-hydroxyquinoline-2-carbaldehyde molecule.

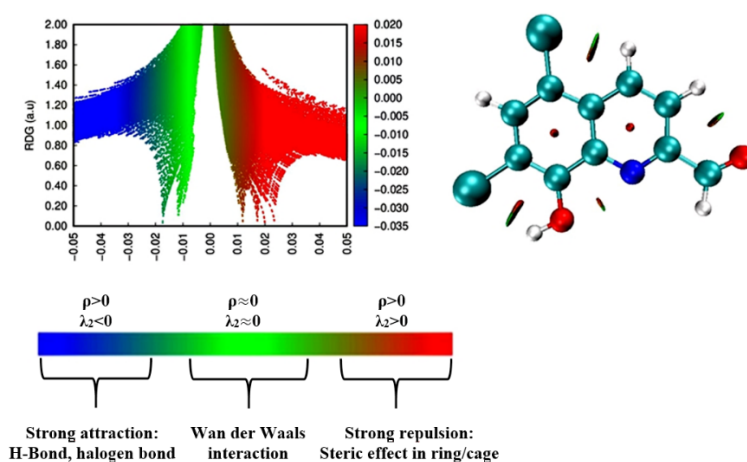


Figure 7. 2D scatter and isosurface density plot of 5,7-dichloro-8-hydroxyquinoline-2-carbaldehyde molecule.

rings, the repulsive effect is observed between 0.02 and 0.05 a.u. values, exhibiting a strong steric effect (red color). In addition, red mixed green flaky patches symbolize the interactions of Van der Waals molecules with each other during this process and show that non-covalent weak C-H...O, O-H...Cl, and N...O interactions occur (Figure 7).

### 3.9. MEP analysis

The molecular electrostatic potential (MEP) diagram is widely recognized for its ability to provide valuable information on the chemical reactivity behavior of medicinal compounds. It allows for accurate predictions of the electrophilic and nucleophilic regions of molecular systems. There are different colors on the molecular electrostatic potential (MEP). The red color shows areas of the molecule with a lot of electrons (negative electrostatic potential regions for nucleophilic attack reactions), and the blue color shows areas with few electrons (positive electrostatic potential regions for electrophilic attack reactions) [42]. The red color on the MEP is typically associated with the presence of a lone pair of electrons on the electronegative atom. In contrast, the blue color of the MEP is indicative of the electropositive atom or group, such as a hydrogen atom or a single-bond CH<sub>3</sub> group [43-45]. The MEP maps obtained from the calculations for the gas phase and other solvents are presented in Figure 8. The most negative value of the electron density of the MEP map in the gas phase is -0.05462 a.u. and the most positive value is +0.05462 a.u. In solvents, the negative values and positive values of electron densities raised with the increase of the dielectric coefficient. In other words,

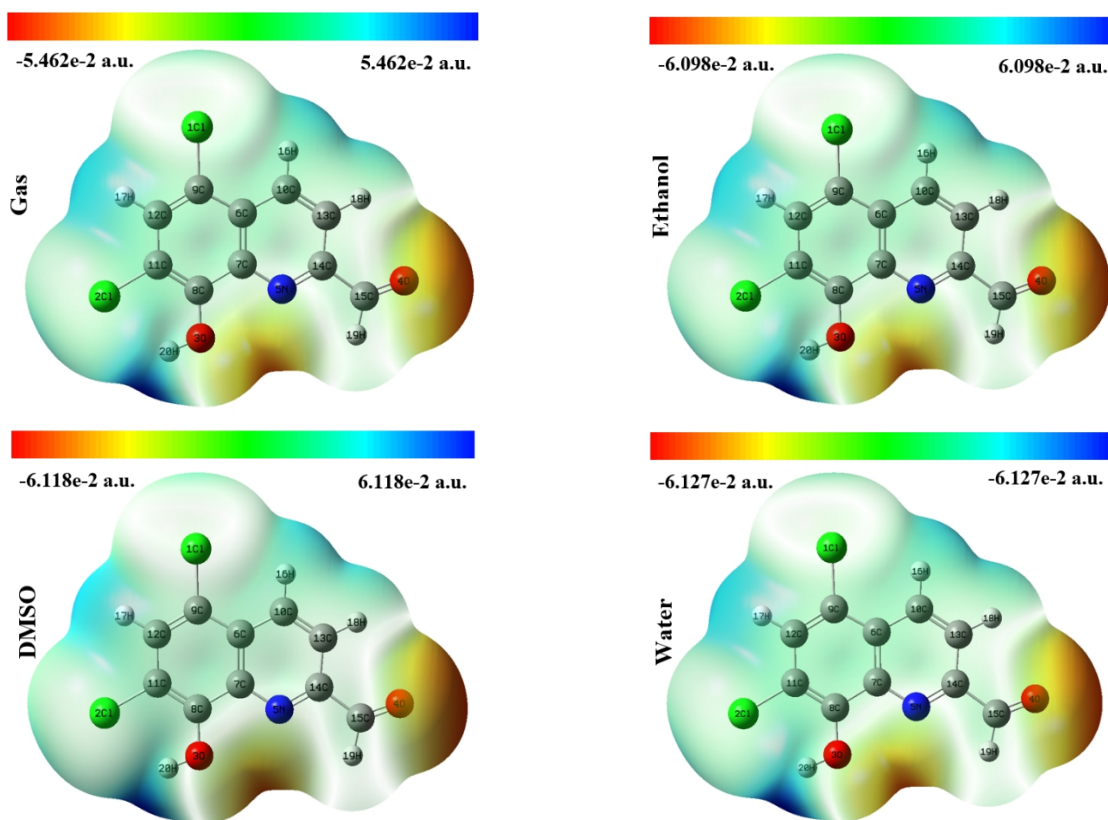
regions with electrophilic properties became more negative, and regions with nucleophilic properties became more positive. The charge distribution of the atoms changed in environments with a dielectric constant higher than that of the gas phase. The reason for the change in charge distribution can be explained as the interaction between the solvent and the solute that is affected by hydrogen bonds and dipole-dipole interactions [34]. When the maps designed for the gas phase and all solvents are examined, it can be said that the most electrophilic regions are the O<sub>4</sub>, O<sub>3</sub>, and N<sub>5</sub> atoms.

### 3.10. Charge analyses

One of the most common methods used to explain electronic properties is to calculate the charge values of the atoms of that molecule [46,47]. Therefore, atomic polar tensor (APT), Hirshfeld, and NBO charge analyses of the optimized 5,7-dichloro-8-hydroxyquinoline-2-carbaldehyde molecule were calculated in the gas phase and in ethanol, DMSO, and water solvents. The charge values are presented in Table 7. In the calculations made in the gas phase, the O<sub>3</sub>, O<sub>4</sub> and N<sub>5</sub> atoms were found to be the atoms with the most negative values in all charge analysis calculations. Compared to the MEP map presented in Figure 8, the results obtained are quite consistent with each other. When the calculations made for other solvents are examined, it is determined that the charge distributions on the atoms of the molecule change with the change of the dielectric constant of the medium, and the negativity of the O<sub>3</sub>, O<sub>4</sub>, and N<sub>5</sub> atoms increases. It was also determined in the MEP map that the negative and positive values in the electron

**Table 7.** Charge values of the 5,7-dichloro-8-hydroxyquinoline-2-carbaldehyde molecule.

Atoms	Gas $\epsilon = 1$			Ethanol $\epsilon = 24.3$			DMSO $\epsilon = 46.8$			Water $\epsilon = 78.3$		
	APT	Hirshfeld	NBO	APT	Hirshfeld	NBO	APT	Hirshfeld	NBO	APT	Hirshfeld	NBO
Cl <sub>1</sub>	-0.314	-0.042	0.030	-0.431	-0.035	0.028	-0.435	-0.035	0.028	-0.437	-0.035	0.028
Cl <sub>2</sub>	-0.331	-0.033	0.034	-0.453	-0.002	0.042	-0.457	-0.001	0.043	-0.459	-0.001	0.043
O <sub>3</sub>	-0.686	-0.172	-0.645	-0.960	-0.199	-0.667	-0.972	-0.200	-0.667	-0.977	-0.200	-0.668
O <sub>4</sub>	-0.778	-0.241	-0.526	-1.085	-0.283	-0.569	-1.097	-0.284	-0.570	-1.102	-0.284	-0.571
N <sub>5</sub>	-0.275	-0.136	-0.384	-0.340	-0.149	-0.409	-0.342	-0.149	-0.410	-0.343	-0.150	-0.410
C <sub>6</sub>	-0.038	-0.012	-0.112	-0.018	-0.010	-0.107	-0.017	-0.010	-0.107	-0.017	-0.010	-0.107
C <sub>7</sub>	0.091	0.050	0.127	0.111	0.047	0.129	0.112	0.047	0.129	0.112	0.047	0.129
C <sub>8</sub>	0.433	0.073	0.332	0.633	0.070	0.330	0.641	0.070	0.330	0.645	0.070	0.330
C <sub>9</sub>	0.276	0.027	-0.025	0.358	0.029	-0.023	0.361	0.029	-0.023	0.362	0.029	-0.023
C <sub>10</sub>	0.051	-0.017	-0.121	0.078	-0.005	-0.111	0.078	-0.005	-0.110	0.079	-0.004	-0.110
C <sub>11</sub>	0.312	0.011	-0.118	0.425	0.018	-0.110	0.428	0.018	-0.110	0.430	0.019	-0.110
C <sub>12</sub>	-0.079	-0.045	-0.211	-0.086	-0.038	-0.204	-0.086	-0.038	-0.203	-0.086	-0.038	-0.203
C <sub>13</sub>	-0.121	-0.026	-0.191	-0.169	-0.021	-0.191	-0.171	-0.021	-0.191	-0.172	-0.021	-0.191
C <sub>14</sub>	-0.073	0.056	0.091	-0.152	0.051	0.088	-0.154	0.051	0.088	-0.155	0.050	0.088
C <sub>15</sub>	0.983	0.139	0.399	1.395	0.137	0.417	1.410	0.137	0.418	1.417	0.137	0.418
H <sub>16</sub>	0.069	0.048	0.227	0.094	0.056	0.235	0.095	0.057	0.236	0.096	0.057	0.236
H <sub>17</sub>	0.092	0.057	0.236	0.118	0.063	0.245	0.119	0.063	0.246	0.119	0.063	0.246
H <sub>18</sub>	0.088	0.059	0.241	0.101	0.063	0.243	0.102	0.063	0.243	0.102	0.063	0.243
H <sub>19</sub>	-0.026	0.045	0.136	-0.040	0.051	0.141	-0.041	0.051	0.141	-0.041	0.051	0.141
H <sub>20</sub>	0.327	0.158	0.477	0.422	0.158	0.491	0.426	0.159	0.492	0.427	0.159	0.492

**Figure 8.** Molecular electrostatic potential surface maps of the 5,7-dichloro-8-hydroxyquinoline-2-carbaldehyde molecule.

density increase. Therefore, the results of the solvent effect obtained in the charge calculations are in accordance with the MEP map. As a result, from the charge calculations for the gas phase and all other solvent environments, it was found that the electrophilic sites that can be subjected to nucleophilic attack are O<sub>3</sub>, O<sub>4</sub>, and N<sub>5</sub> atoms.

### 3.11. ELF (electron localization function) and LOL (localized orbital locator) analysis

ELF and LOL maps obtained from covalent bond-based surface analysis were created using the Multiwfn software program [18]. These maps reveal regions on the molecular surface where the probability of finding an electron pair is high.

The ELF and LOL have a chemical composition that is similar because of their dependence on the kinetic energy density. However, ELF is derived from the density of electron pairs, while LOL is typically observed when localized orbitals overlap, resulting in high gradients of localized orbitals [48]. ELF and LOL images of the title molecule are depicted in a color tint map and contour map in the ranges of 0.0 to 1.0 and 0.0 to 0.8, respectively, in Figures 9 and 10. The interval of 0.5-1.0 is characterized by the presence of localized electrons that are both bonding and nonbonding, while delocalized electrons are anticipated in the smaller interval (< 0.5) [49]. When the ELF maps designed for the gas phase and other solvents are examined, it is seen that the bound and unbound localized electrons are concentrated, especially on the H<sub>16</sub>, H<sub>17</sub>, H<sub>18</sub>,

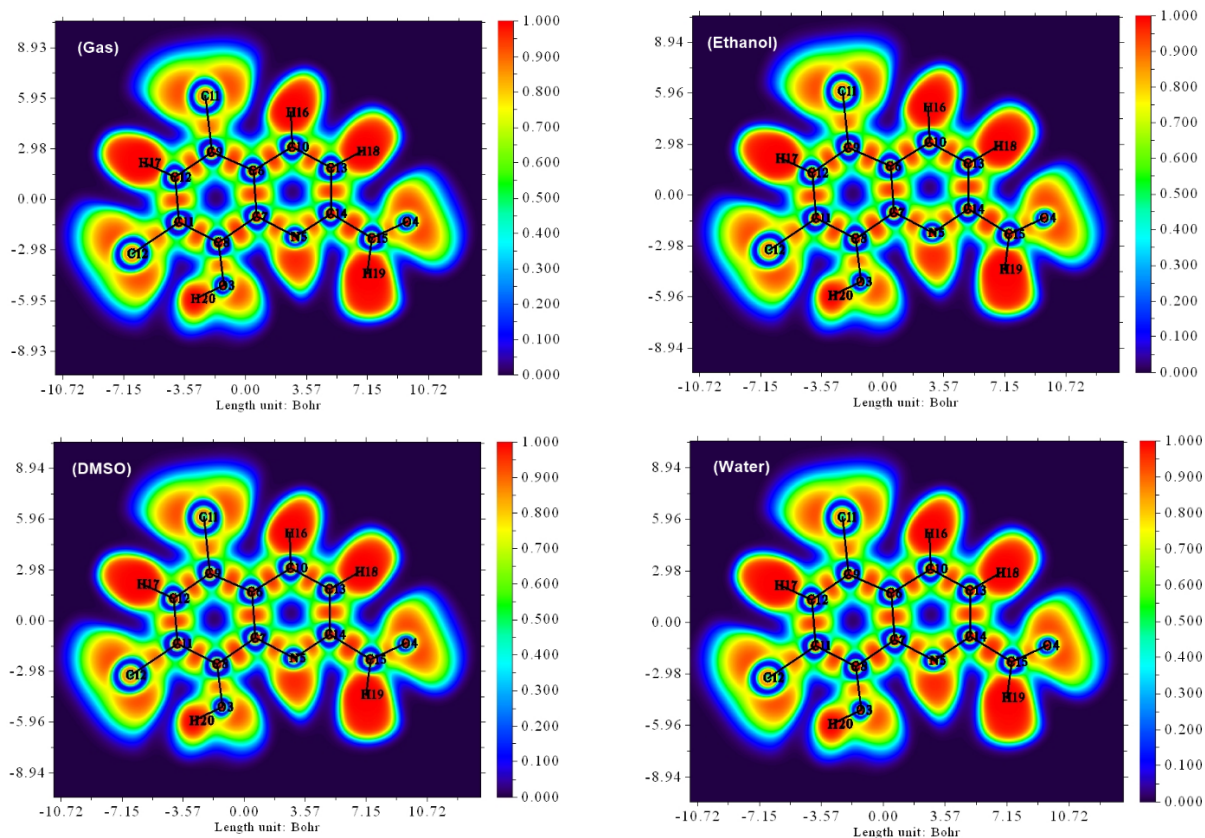


Figure 9. ELF maps of the 5,7-dichloro-8-hydroxyquinoline-2-carbaldehyde molecule.

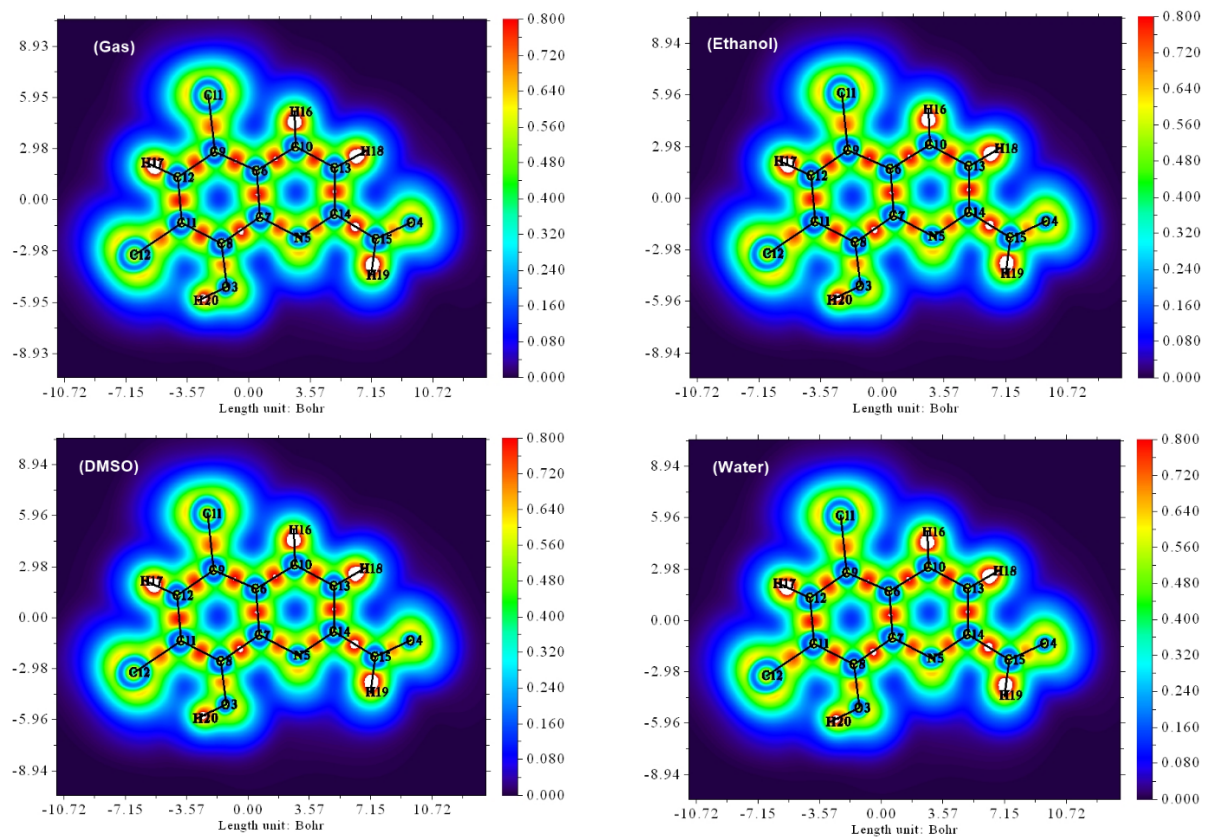


Figure 10. LOL maps of the 5,7-dichloro-8-hydroxyquinoline-2-carbaldehyde molecule.

**Table 8.** The electric dipole moment  $\mu$  (Debye), average polarizability  $\bar{\alpha}$ , anisotropy of polarizability  $\Delta\alpha$  ( $10^{-24}$  esu), and first hyperpolarizability  $\beta$  ( $10^{-30}$  esu) of the 5,7-dichloro-8-hydroxyquinoline-2-carbaldehyde molecule in the gas phase and solvents.

Parameters	Gas $\epsilon = 1$	Ethanol $\epsilon = 24.3$	DMSO $\epsilon = 46.8$	Water $\epsilon = 78.3$
$\mu_x$	-1.332	-4.422	-4.458	-4.475
$\mu_y$	0.260	1.077	1.097	1.107
$\mu_z$	0.303	0.000	0.000	0.00009
$\mu$	1.332	4.550	4.591	4.611
$\alpha_{xx}$	36.237	51.005	51.533	51.78
$\alpha_{yy}$	0.528	0.865	0.875	0.881
$\alpha_{zz}$	26.42	36.787	37.187	37.373
$\alpha_{xy}$	0.00033	0.00051	0.00051	0.00051
$\alpha_{yz}$	-0.00025	-0.00037	-0.00038	-0.00038
$\alpha_{zx}$	11.308	15.033	15.251	15.356
$\bar{\alpha}$	24.655	34.275	34.657	34.836
$\Delta\alpha$	21.770	31.415	31.686	31.809
$\beta_{xxx}$	10.478	33.571	34.733	35.283
$\beta_{xyx}$	-0.304	-0.792	-0.802	-0.806
$\beta_{yyx}$	1.288	3.655	3.781	3.841
$\beta_{yxy}$	-0.119	-0.758	-0.821	-0.851
$\beta_{xzz}$	0.00045	11.911	0.0013	0.00124
$\beta_{yyz}$	-0.00006	-0.00017	-0.00018	-0.00018
$\beta_{yyz}$	-0.00001	-0.00003	-0.00003	-0.00004
$\beta_{zzz}$	-0.0794	-0.123	-0.128	-0.128
$\beta_{zyz}$	0.285	0.605	0.625	0.635
$\beta_{zzz}$	0.00008	0.00009	0.00009	0.00009
$\beta_x$	11.687	37.103	38.386	38.996
$\beta_y$	-0.138	-0.945	-0.998	-1.022
$\beta_z$	0.001	11.911	0.001	0.001
$\beta_{tot}$	11.687	38.979	38.399	39.009
$\beta$	0.0003	7.1466	0.0008	0.0008

$$\mu^2 = \mu_x^2 + \mu_y^2 + \mu_z^2 \quad (2)$$

$$\bar{\alpha} = (\alpha_{xx} + \alpha_{yy} + \alpha_{zz}) / 3 \quad (3)$$

$$\Delta\alpha = \frac{1}{\sqrt{2}} [(\alpha_{xx} - \alpha_{yy})^2 + (\alpha_{yy} - \alpha_{zz})^2 + (\alpha_{zz} - \alpha_{xx})^2 + 6(\alpha_{xy}^2 + \alpha_{yz}^2 + \alpha_{zx}^2)]^{1/2} \quad (4)$$

$$\beta_0 = [(\beta_{xxx} + \beta_{yyy} + \beta_{zzz})^2 + (\beta_{yyy} + \beta_{xyx} + \beta_{yxy})^2 + (\beta_{zzz} + \beta_{xzx} + \beta_{zyz})^2]^{1/2} \quad (5)$$

H19, and H20 atoms. The unlocalized electrons are determined to be concentrated in the O3, O4, N5, Cl11, C12, and C atoms. The LOL map also presents similar results with the ELF map. When these two maps are compared with the MEP map and charge analysis, similar results are obtained. In the MEP map and charge analysis, the O3, O4 and N5 atoms were found in the electrophilic region. The increase in the dielectric coefficient in the solvent environments only affected the electron charge distribution and did not cause any change in the electrophilic and nucleophilic regions. In other words, it was determined that the solvent effect did not have a significant effect on the ELF and LOL of the title molecule [50].

### 3.12. Nonlinear optical property analysis

Advanced technological applications such as frequency shifting, optical modulation, switching, lasers, fiber optic materials, and optical memory utilize nonlinear optical materials. Therefore, the search for materials with non-linear optical characteristics has recently become common and significant [51]. The interaction between an electron-donating group and an electron-withdrawing group links the first hyperpolarizability value to the alteration in the conjugation length. Increasing or decreasing conjugation length can change the strength of second-order nonlinear optical (NLO) responses [52]. The permanent dipole moment ( $\mu$ ), average polarizability, the anisotropy of the polarizability, and the first-order hyperpolarizability values were calculated using Equations 2-4 [53,54].

Table 8 presents the results obtained for the gas phase, ethanol, DMSO, and water solvents. Urea, which has been

shown to be the standard molecule in the literature, is used to evaluate the results. The dipole moment and the first hyperpolarizability values of this molecule are 1.3732 D and  $0.3728 \times 10^{-30}$  esu [55]. In the calculations performed in the gas phase of the title molecule, the dipole moment value was found to be 1.332 D. This parameter value was found to be 4.550, 4.591, and 4.611 D for ethanol, DMSO, and water solvents, respectively. The first hyperpolarizability values were calculated as  $11.687 \times 10^{-30}$ ,  $38.979 \times 10^{-30}$ ,  $38.399 \times 10^{-30}$ , and  $39.009 \times 10^{-30}$  esu for the gas phase, ethanol, DMSO, and water solvents, respectively. These values in the solvent are much higher than those of the urea. The identification of this compound is essential because it can be employed as NLO in further studies.

### 4. Conclusions

In this study, the most stable conformer structure of 5,7-dichloro-8-hydroxyquinoline-2-carbaldehyde was found using the MMMF theory in the Spartan 08 package program. Then, the optimized geometric structure of this conformer structure was determined by the DFT method, and its spectroscopic and electronic properties were investigated. This study aims to investigate how much of a shift will occur in solvent environments according to the results obtained in the gas phase in infrared, UV-vis, and NMR ( $^1\text{H}$  and  $^{13}\text{C}$ ) spectra. The results show that the effects of solvents on the vibration and UV-vis spectra of the compound are almost the same. In the  $^1\text{H}$  NMR values, only some of the values calculated in a water environment changed significantly compared to the other two solvents. Analysis of FMO, TDOS, and PDOS spectra showed

charge transfer in the compound. The surface and atomic charges of MEP confirmed the areas where electrophilic and nucleophilic attacks could occur, *i.e.*, at reactive sites of the title molecule. NCI-RDG analysis showed weak and strong attractive interactions as well as steric repulsions within the molecule. The results obtained from ELF and LOL analyses also support the results obtained from NCI analysis. NBO analysis revealed donor-acceptor interactions and electron transfer interactions in the 5,7-dichloro-8-hydroxyquinoline-2-carbaldehyde molecule. Furthermore, the first-order hyperpolarizability is significantly higher than that of urea in gases and solvents, suggesting that the studied molecule is suitable for NLO applications.

## Acknowledgements

The author is grateful to Prof. Omer DERELI for providing use of the Spartan 08 package program.

## Disclosure statement

Conflict of interest: The authors declare that they have no conflict of interest. Ethical approval: All ethical guidelines have been adhered to. Sample availability: Samples of the compounds are available from the author.

## ORCID and Email

Ceyhun Kucuk

[ceyhun.kucuk@beun.edu.tr](mailto:ceyhun.kucuk@beun.edu.tr)

<https://orcid.org/0000-0003-4457-8798>

## References

- Zhang, W.; He, X.; Deng, N.; Wang, Y.; He, J. Monitoring of intermediates of cloquinol electro-oxidation by thin-layer spectral and electrophoretic electrochemistry. *Electrochim. Acta* **2014**, *127*, 403–409.
- Rohde, W.; Mikelens, P.; Jackson, J.; Blackman, J.; Whitcher, J.; Levinson, W. Hydroxyquinolines Inhibit Ribonucleic Acid-Dependent Deoxyribonucleic Acid Polymerase and Inactivate Rous Sarcoma Virus and Herpes Simplex Virus. *Antimicrob Agents Chemother* **1976**, *10* (2), 234–240.
- Fischer, T.; Hartvig, P. Skin absorption of 8-hydroxyquinolones. *Lancet* **1977**, *309* (8011), 603.
- Gholz, L. M.; Arons, W. L. Prophylaxis and Therapy of Amebiasis and Shigellosis with Iodochlorhydroxyquin. *Am. J. Trop. Med. Hyg.* **1964**, *13* (3), 396–401.
- Martínez-Larrañaga, M. R.; Anadón, A.; Fernandez-Cruz, M. L.; Díaz, M. J.; Martínez, M. A.; Frejo, M. T.; Martínez, M.; Tafur, M. Cytotoxicity in pig hepatocytes induced by 8-quinolinol, chloramine-T and natamycin. *Vet. Pharm. & Therapeutics* **2000**, *23* (1), 37–44.
- Sureshkumar, B.; Mary, Y. S.; Mary, Y. S.; Suma, S. Spectroscopic and DFT investigations of 8-hydroxy quinoline-5-sulfonic acid-5-chloro-8-hydroxyquinoline cocrystal. *Chem. Pap.* **2021**, *75* (7), 3387–3399.
- Agwupuye, J. A.; Gber, T. E.; Edet, H. O.; Zeeshan, M.; Batool, S.; Duke, O. E.; Adah, P. O.; Odey, J. O.; Egbung, G. E. Molecular modeling, DFT studies and biological evaluation of methyl 2,8-dichloro-1,2-dihydroquinoline-3-carboxylate. *Chem. Phys. Impact* **2023**, *6*, 100146.
- Chaturvedi, G.; Kaur, A.; Umar, A.; Khan, M. A.; Algarni, H.; Kansal, S. K. Removal of fluoroquinolone drug, levofloxacin, from aqueous phase over iron based MOFs, MIL-100(Fe). *J. Solid State Chem.* **2020**, *281*, 121029.
- Lgaz, H.; Salghi, R.; Subrahmanya Bhat, K.; Chaouiki, A.; Shubhalaxmi; Jodeh, S. Correlated experimental and theoretical study on inhibition behavior of novel quinoline derivatives for the corrosion of mild steel in hydrochloric acid solution. *J. Mol. Liq.* **2017**, *244*, 154–168.
- Lakshmi, A.; Balachandran, V.; Janaki, A. Comparative vibrational spectroscopic studies, HOMO–LUMO and NBO analysis of 5,7-dibromo-8-hydroxyquinoline and 5,7-dichloro-8-hydroxyquinoline based on Density Functional Theory. *J. Mol. Struct.* **2011**, *1004* (1-3), 51–66.
- Shao, Y.; Molnar, L. F.; Jung, Y.; Kussmann, J.; Ochsenfeld, C.; Brown, S. T.; Gilbert, A. T.; Slipchenko, L. V.; Levchenko, S. V.; O'Neill, D. P.; DiStasio Jr, R. A.; Lochan, R. C.; Wang, T.; Beran, G. J.; Besley, N. A.; Herbert, J. M.; Yeh Lin, C.; Van Voorhis, T.; Hung Chien, S.; Sodt, A.; Steele, R. P.; Rassolov, V. A.; Maslen, P. E.; Korambath, P. P.; Adamson, R. D.; Austin, B.; Baker, J.; Byrd, E. F.; Dachsel, H.; Doerksen, R. J.; Dreuw, A.; Dunietz, B. D.; Dutoi, A. D.; Furlani, T. R.; Gwaltney, S. R.; Heyden, A.; Hirata, S.; Hsu, C.; Kedziora, G.; Khalliulin, R. Z.; Klunzinger, P.; Lee, A. M.; Lee, M. S.; Liang, W.; Lotan, I.; Nair, N.; Peters, B.; Proynov, E. I.; Pieniazek, P. A.; Min Rhee, Y.; Ritchie, J.; Rosta, E.; David Sherrill, C.; Simmonett, A. C.; Subotnik, J. E.; Lee Woodcock III, H.; Zhang, W.; Bell, A. T.; Chakraborty, A. K.; Chipman, D. M.; Keil, F. J.; Warshel, A.; Hehre, W. J.; Schaefer III, H. F.; Kong, J.; Krylov, A. I.; Gill, P. M.; Head-Gordon, M. Advances in methods and algorithms in a modern quantum chemistry program package. *Phys. Chem, Chem, Phys.* **2006**, *8* (27), 3172–3191.
- GaussView, Version 5, Dennington, R.; Keith, T. A.; Millam, J. M. Semicem Inc., Shawnee Mission, KS, 2009.
- Becke, A. D. Density-functional thermochemistry. III. The role of exact exchange. *J. Chem. Phys.* **1993**, *98* (7), 5648–5652.
- Frisch, M. J.; Trucks, G. W.; Schlegel, H. B.; Scuseria, G. E.; Robb, M. A.; Cheeseman, J. R.; Montgomery, J. A.; Vreven, T.; Kudin, K. N.; Burant, J. C.; Millam, J. M.; Iyengar, S. S.; Tomasi, J.; Barone, V.; Mennucci, B.; Cossi, M.; Scalmani, G.; Rega, N.; Petersson, G. A.; Nakatsuji, H.; Hada, M.; Ehara, M.; Toyota, K.; Fukuda, R.; Hasegawa, J.; Ishida, M.; Nakajima, T.; Honda, Y.; Kitao, O.; Nakai, H.; Klene, M.; Li, X.; Knox, J. E.; Hratchian, H. P.; Cross, J. B.; Adamo, C.; Jaramillo, J.; Gomperts, R.; Stratmann, R. E.; Yazyev, O.; Austin, A. J.; Cammi, R.; Pomelli, C.; Ochterski, J. W.; Ayala, P. Y.; Morokuma, K.; Voth, G. A.; Salvador, P.; Dannenberg, J. J.; Zakrzewski, V. G.; Dapprich, S.; Daniels, A. D.; Strain, M. C.; Farkas, O.; Malick, D. K.; Rabuck, A. D.; Raghavachari, K.; Foresman, J. B.; Ortiz, J. V.; Cui, Q.; Baboul, A. G.; Clifford, S.; Cioslowski, J.; Stefanov, B. B.; Liu, G.; Liashenko, A.; Piskorz, P.; Komaromi, I.; Martin, R. L.; Fox, D. J.; Keith, T.; Al-Laham, M. A.; Peng, C. Y.; Nanayakkara, A.; Challacombe, M.; Gill, P. M. W.; Johnson, B.; Chen, W.; Wong, M. W.; Gonzalez, C.; Pople, J. A. Gaussian 09, Gaussian, Inc., Wallingford CT, 2004.
- Erdogdu, Y.; Başköse, Ü. C.; Sağlam, S. Conformational, structural, electronic, and vibrational investigations on 5-methyl-4-(2-thiazolylazo)resorcinol by FT-IR, FT-Raman, NMR, and DFT. *Chem. Pap.* **2019**, *73* (8), 1879–1891.
- Kucuk, C.; Yurdakul, S.; Özdemir, N.; Erdem, B. Structural and spectroscopic characterization, electronic properties, and biological activity of the 4-(3-methoxyphenyl)piperazin-1-ium 4-(3-methoxy phenyl)piperazine-1-carboxylate monohydrate. *Chem. Pap.* **2023**, *77* (5), 2793–2815.
- Subashini, K.; Periandy, S. Spectroscopic (FT-IR, FT-Raman, UV, NMR, NBO) investigation and molecular docking study of (R)-2-Amino-1-PhenylEthanol. *J. Mol. Struct.* **2016**, *1117*, 240–256.
- Silvi, B.; Savin, A. Classification of chemical bonds based on topological analysis of electron localization functions. *Nature* **1994**, *371* (6499), 683–686.
- Kucuk, C.; Celik, S.; Yurdakul, S.; Erdem, B. Spectroscopic characterization, DFT calculations, antimicrobial activity, and molecular docking studies of 5-methoxy-1H-benzo[d]imidazole and its Ag(I) complex. *Polyhedron* **2024**, *251*, 116868.
- Disli, A.; Yucesoy, E. E.; Erdogdu, Y.; Gulluoglu, M. T.; Ozturk, A.; Dilek, G. Synthesis, characterization, theoretical studies and antimicrobial activity of novel 1-(2-hydroxy-4-propoxy-3-propylphenyl)ethanones bearing thiotetrazole. *J. Mol. Struct.* **2021**, *1242*, 130818.
- Ravindranath, L.; Reddy, B. V. Theoretical and experimental study of torsional potentials, molecular structure (monomer and dimer), vibrational analysis and molecular characteristics of some dimethyl bipyridines. *J. Mol. Struct.* **2020**, *1200*, 127089.
- Ma, Z.; Moulton, B. 5-Chloro-8-hydroxyquinoline; Experimental Crystal Structure Determination. CCDC. 2010, 687619 <https://doi.org/10.5517/ccr2j8l>
- Pieczka, A.; Ertl, A.; Gołębiewska, B.; Jeleń, P.; Kotowski, J.; Nejbart, K.; Stachowicz, M.; Giester, G. Crystal structure and Raman spectroscopic studies of OH stretching vibrations in Zn-rich fluor-elbaite. *Am. Mineral.* **2020**, *105* (11), 1622–1630.
- Sureshkumar, B.; Sheena Mary, Y.; Suma, S.; Armaković, S.; Armaković, S. J.; Alsenoy, C. V.; Narayana, B.; Sasidharan, B. P. Spectroscopic characterization of 8-hydroxy-5-nitroquinoline and 5-chloro-8-hydroxy quinoline and investigation of its reactive properties by DFT calculations and molecular dynamics simulations. *J. Mol. Struct.* **2018**, *1164*, 525–538.
- Arivazhagan, R.; Sridevi, C.; Prakasam, A. Exploring molecular structure, spectral features, electronic properties and molecular docking of a novel biologically active heterocyclic compound 4-phenylthiosemicarbazide. *J. Mol. Struct.* **2021**, *1232*, 129956.
- Yurdakul, Ş.; Badoğlu, S.; Güleşçi, Y. Experimental and theoretical study on free 5-nitroquinoline, 5-nitroquinoline, and their zinc(II) halide complexes. *Spectrochim. Acta A: Mol. Biomol. Spectrosc.* **2015**, *137*, 945–956.
- Ling, Y.; Huang, L.; Hong, W.; Liu, T.; Luan, J.; Liu, W.; Lai, J.; Li, H. Polarization-controlled dynamically switchable plasmon-induced transparency in plasmonic metamaterial. *Nanoscale* **2018**, *10* (41), 19517–19523.
- Ulahannan, R.; Kannan, V.; Vidya, V.; Sreekumar, K. Synthesis and DFT studies of the structure - NLO activity evaluation of 2-(4-methoxy

- phenyl)-1,4,5-triphenyl-2,5-dihydro-1H-imidazole. *J. Mol. Struct.* **2020**, *1199*, 127004.
- [29]. Selvaraj, S.; Rajkumar, P.; Kesavan, M.; Gunasekaran, S.; Kumaresan, S. Experimental and theoretical investigations on spectroscopic properties of tropicamide. *J. Mol. Struct.* **2018**, *1173*, 52–62.
- [30]. Yurdakul, S.; Tanrıbuurdu, S. Theoretical and experimental study of solvent effects on the structure, vibrational spectra, and tautomerism of 3-amino-1,2,4-triazine. *J. Mol. Struct.* **2013**, *1052*, 57–66.
- [31]. Hiremath, S. M.; Suvitha, A.; Patil, N. R.; Hiremath, C. S.; Khemalapur, S. S.; Pattanayak, S. K.; Negalurmath, V. S.; Obelannavar, K. Molecular structure, vibrational spectra, NMR, UV, NBO, NLO, HOMO-LUMO and molecular docking of 2-(4, 6-dimethyl-1-benzofuran-3-yl) acetic acid (2DBAA): Experimental and theoretical approach. *J. Mol. Struct.* **2018**, *1171*, 362–374.
- [32]. Beatrice, M. L.; Delphine, S. M.; Amalanathan, M.; Mary, M. S.; Robert, H. M.; Mol, K. T. Molecular structure, spectroscopic, Fukui function, RDG, anti-microbial and molecular docking analysis of higher concentration star anise content compound methyl 4-methoxy benzoate-DFT study. *J. Mol. Struct.* **2021**, *1238*, 130381.
- [33]. Kucuk, C.; Celik, S.; Yurdakul, S.; Coteli, E. A new Ag(I)-complex of 5-chloroquinolin-8-ol ligand: Synthesis, spectroscopic characterization, and DFT investigations, in vitro antioxidant (DPPH and ABTS),  $\alpha$ -glucosidase,  $\alpha$ -amylase inhibitory activities with protein-binding analysis. *J. Mol. Struct.* **2025**, *1325*, 141285.
- [34]. Khodiev, M.; Holikulov, U.; Jumabaev, A.; ISSAOUI, N.; Nikolay Lvovich, L.; Al-Dossary, O. M.; Bousiakoug, L. G. Solvent effect on the self-association of the 1,2,4-triazole: A DFT study. *J. Mol. Liq.* **2023**, *382*, 121960.
- [35]. Chen, R.; Li, Q.; Zhang, Z.; Xu, K.; Sun, L.; Ma, J.; Wang, T.; Mu, X.; Xi, Y.; Cao, L.; Teng, B.; Wu, H. Solvent effect on ESIPT process of N-(8-Quinoly) salicylaldehyde: A DFT/TD-DFT calculation. *J. Photochem. Photobiol. A: Chem.* **2023**, *436*, 114335.
- [36]. Makhlof, J.; Louis, H.; Benjamin, I.; Ukwenya, E.; Valkonen, A.; Smirani, W. Single crystal investigations, spectral analysis, DFT studies, antioxidants, and molecular docking investigations of novel hexaammoniochromate complex. *J. Mol. Struct.* **2023**, *1272*, 134223.
- [37]. Vincy, C. D.; Tarika, J. D.; Dextrin, X. D.; Rathika, A.; Beaula, T. J. Exploring the antibacterial activity of 1, 2 diaminoethane hexanedionic acid by spectroscopic, electronic, ELF, LOL, RDG analysis and molecular docking studies using DFT method. *J. Mol. Struct.* **2022**, *1247*, 131388.
- [38]. Celik, S.; Yurdakul, S.; Erdem, B. New silver(I) complex as antibiotic candidate: Synthesis, spectral characterization, DFT, QAIM and antibacterial investigations and docking properties. *J. Mol. Struct.* **2022**, *1261*, 132902.
- [39]. Sakr, M. A.; Saad, M. A. Spectroscopic investigation, DFT, NBO and TD-DFT calculation for porphyrin (PP) and porphyrin-based materials (PPBMs). *J. Mol. Struct.* **2022**, *1258*, 132699.
- [40]. Mazumdar, P.; Choudhury, D. Study of the alkyl- $\pi$  interaction between methane and few substituted pyrimidine systems using DFT, AIM and NBO calculations. *Comput. Theor. Chem.* **2022**, *1208*, 113560.
- [41]. Medimagh, M.; Issaoui, N.; Gafsaoui, S.; Kazachenko, A. S.; Al-Dossary, O. M.; Kumar, N.; Marouani, H.; Bousiakoug, L. G. Investigations on the non-covalent interactions, drug-likeness, molecular docking and chemical properties of 1,1,4,7,7-pentamethyldiethylenetri ammonium trinitrate by density-functional theory. *J. King Saud Univ. - Sci.* **2023**, *35* (4), 102645.
- [42]. Kucuk, C.; Celik, S.; Yurdakul, S.; Coteli, E.; Erdem, B. Synthesis, characterization, thermal, DFT study, antioxidant and antimicrobial in vitro investigations of indazole and its Ag(I) complex. *Polyhedron* **2023**, *241*, 116469.
- [43]. Uludağ, N.; Serdaroğlu, G. An improved synthesis, spectroscopic (FT-IR, NMR) study and DFT computational analysis (IR, NMR, UV-Vis, MEP diagrams, NBO, NLO, FMO) of the 1,5-methanoazocino[4,3-b]indole core structure. *J. Mol. Struct.* **2018**, *1155*, 548–560.
- [44]. Suhta, A.; Saral, S.; Çoruh, U.; Karakuş, S.; Vazquez-Lopez, E. M. Synthesis, Single Crystal X-Ray, Hirshfeld Surface Analysis and DFT Calculation Based NBO, HOMO-LUMO, MEP, ECT and Molecular Docking Analysis of N'-[[2,6-Dichlorophenyl]Methylidene]-2-[[3-(Trifluoromethyl)Phenyl]Amino]Benzohydrazide. *J. Struct. Chem.* **2024**, *65* (1), 196–215.
- [45]. Kargar, H.; Fallah-Mehrjardi, M.; Behjatmanesh-Ardakani, R.; Munawar, K. S.; Ashfaq, M.; Tahir, M. N. Diverse coordination of isoniazid hydrazone Schiff base ligand towards iron(III): Synthesis, characterization, SC-XRD, HSA, QAIM, MEP, NCI, NBO and DFT study. *J. Mol. Struct.* **2022**, *1250*, 131691.
- [46]. Kucuk, C. Synthesis, characterization, DFT studies, and molecular docking investigation of silver nitrate complex of 5-benzimidazole carboxylic acid as targeted anticancer agents. *J. Mol. Struct.* **2023**, *1293*, 136166.
- [47]. Celik, S.; Alp, M.; Yurdakul, S. A combined experimental and theoretical study on vibrational spectra of 3-pyridyl methyl ketone. *Spectrosc. Lett.* **2020**, *53* (4), 234–248.
- [48]. Janani, S.; Rajagopal, H.; Muthu, S.; Aayisha, S.; Raja, M. Molecular structure, spectroscopic (FT-IR, FT-Raman, NMR), HOMO-LUMO, chemical reactivity, AIM, ELF, LOL and Molecular docking studies on 1-Benzyl-4-(N-Boc-amino)piperidine. *J. Mol. Struct.* **2021**, *1230*, 129657.
- [49]. Khemalapur, S. S.; Katti, V. S.; Hiremath, C. S.; Hiremath, S. M.; Basanagouda, M.; Radder, S. B. Spectroscopic (FT-IR, FT-Raman, NMR and UV-Vis), ELF, LOL, NBO, and Fukui function investigations on (5-bromo-benzofuran-3-yl)-acetic acid hydrazide (5BBAH): Experimental and theoretical approach. *J. Mol. Struct.* **2019**, *1196*, 280–290.
- [50]. Thirunavukkarasu, M.; Prabakaran, P.; Saral, A.; Alharbi, N. S.; Kadaikunnan, S.; Kazachenko, A. S.; Muthu, S. Molecular level solvent interaction (microscopic), electronic, covalent assembly (RDG, AIM & ELF), ADMET prediction and anti-cancer activity of 1-(4-Fluorophenyl)-1-propanone: Cytotoxic agent. *J. Mol. Liq.* **2023**, *380*, 121714.
- [51]. Altürk, S.; Tamer, Ö.; Avci, D.; Atalay, Y. Synthesis, spectroscopic characterization, second and third-order nonlinear optical properties, and DFT calculations of a novel Mn(II) complex. *J. Organomet. Chem.* **2015**, *797*, 110–119.
- [52]. Lescos, L.; Sitkiewicz, S. P.; Beaujean, P.; Blanchard-Desce, M.; Champagne, B.; Matito, E.; Castet, F. Performance of DFT functionals for calculating the second-order nonlinear optical properties of dipolar merocyanines. *Phys. Chem. Chem. Phys.* **2020**, *22* (29), 16579–16594.
- [53]. Zhang, R.; Du, B.; Sun, G.; Sun, Y. Experimental and theoretical studies on o-, m- and p-chlorobenzylideneaminoantipyridines. *Spectrochim. Acta A: Mol. Biomol. Spectrosc.* **2010**, *75* (3), 1115–1124.
- [54]. Karamanis, P.; Pouchan, C.; Maroulis, G. Structure, stability, dipole polarizability and differential polarizability in small gallium arsenide clusters from all-electron *ab initio* and density-functional-theory calculations. *Phys. Rev. A.* **2008**, *77* (1), <https://doi.org/10.1103/PhysRevA.77.013201>.
- [55]. Sethi, A.; Singh, R. P.; Shukla, D.; Singh, P. Synthesis of novel pregnenediosgenin prodrugs via Ring A and Ring A connection: A combined experimental and theoretical studies. *J. Mol. Struct.* **2016**, *1125*, 616–623.



Copyright © 2025 by Authors. This work is published and licensed by Atlanta Publishing House LLC, Atlanta, GA, USA. The full terms of this license are available at <https://www.eurjchem.com/index.php/eurjchem/terms> and incorporate the Creative Commons Attribution-Non Commercial (CC BY NC) (International, v4.0) License (<http://creativecommons.org/licenses/by-nc/4.0>). By accessing the work, you hereby accept the Terms. This is an open access article distributed under the terms and conditions of the CC BY NC License, which permits unrestricted non-commercial use, distribution, and reproduction in any medium, provided the original work is properly cited without any further permission from Atlanta Publishing House LLC (European Journal of Chemistry). No use, distribution, or reproduction is permitted which does not comply with these terms. Permissions for commercial use of this work beyond the scope of the License (<https://www.eurjchem.com/index.php/eurjchem/terms>) are administered by Atlanta Publishing House LLC (European Journal of Chemistry).